Mechanical Integrity of Spent Nuclear Fuel: From Experimental to Numerical Studies

E. VLASSOPOULOS, A. PAUTZ

Laboratory of Reactor Physics and Systems Behaviour, Swiss Federal Institute of Technology Lausanne

Route Cantonale, 1015 Lausanne – Switzerland

D. PAPAIOANNOU, L. FONGARO, R. NASYROW, R. GRETTER, J. SOMERS, V.V. RONDINELLA

G.III – Nuclear Decommissioning, Joint Research Centre, European Commission

Hermann-von-Helmholtz-Platz 1, 76344 Eggenstein-Leopoldshafen – Germany

S. CARUSO, V. RAFFUZZI, P. GRÜNBERG

Safety, Geology & Radioactive Materials, National Cooperative for the Disposal of Radioactive Waste

Hardstrasse 73, 5430 Wettingen – Switzerland

J. HELFENSTEIN, P. SCHWIZER

CADFEM (Suisse) AG

Wittenwilerstrasse 25, 8355 Aadorf, Switzerland

ABSTRACT

This paper presents the methodology applied to model experimental investigations on the mechanical response of the used nuclear fuel rods under static and dynamic loads. The experimental activities were conducted at the JRC Karlsruhe where a 3-point bending device and an impact tower have been developed and commissioned at the hot-cell facilities. The impact (or crash) was recorded using a high-speed camera, while an image analysis methodology was developed to understand the sample's behaviour under dynamic load. Finite Element Analysis (FEA) was used to simulate the rod's response based on Static and Transient Structural models in ANSYS Mechanical. The models were calibrated against the experimental data using the "optiSLang" approach. Finally, a sensitivity analysis was performed to determine the relative importance of the various model parameters introduced (material properties, geometrical configuration, etc.).

1. Introduction

The options considered for the back-end of the nuclear fuel cycle vary world-wide. One of the most distinctive options is prolonged interim storage of the Spent Nuclear Fuel (SNF) before

its final disposal. Currently, most SNF is kept safely in storage either at on-site facilities or at centralized interim storage sites. Nevertheless, many countries face delays in the implementation of their waste management programmes for SNF and high-level waste (HLW) disposal. As a result, the size of storage sites is being increased, since storage pools are approaching their capacity. Inevitably, an increasing demand for dry-storage solutions is foreseen in the near future [1,2].

In recent years, emerging regulatory issues associated to dry storage of SNF are arising, and can be attributed mainly to two main reasons. The first is simply due to the need of a better understanding of the ageing mechanisms, complemented by experimental data, affecting the properties of the SNF rods during prolonged dry storage conditions [3,4]. The second is connected to the inevitable need of prolonging the storage of SNF in interim facilities [1] for time periods far beyond that originally envisaged, even to more than 100 years. In many cases, Transport and Storage Casks (TSC) and/or interim storage facilities are currently licensed for time periods shorter than now envisaged long interim storage periods.

A multiyear project has been developed by NAGRA, in cooperation with the Joint Research Centre (JRC) and the Swiss Federal Institute of Technology in Lausanne (EPFL) to enrich the knowledge and database underpinning the ageing mechanisms [5]. The objective is to provide a better, if not full, understanding of the phenomena and interactions that affect the potential degradation of SNF rods [3,4,6–8]. Assessments of the consequences of a fuel rod failure are foreseen to provide valuable input data for the optimisation of the SNF and TSC management actions required for their safe handling and disposal.

In particular, this study investigates, experimentally and numerically, the mechanical response of irradiated nuclear fuel rods to mechanical solicitations. The experimental activities are conducted in JRC-Karlsruhe and include a set of mechanical tests on surrogate and irradiated SNF rod segments. Finite Element Analysis (FEA) is used to simulate the rod's behaviour as recorded during the mechanical tests. Determination of the mechanical properties of the fuel/cladding system, derivation of rod failure criteria, optimisation of the material models and examination of the effect of various phenomena (burnup, gap size, strain rate, etc.) represent the main objectives of the numerical studies.

This paper describes test-to-model methodologies applied as a prior task to derive the rod's response in dynamic loads and to validate and optimize the FE models against the experimental results. High speed imaging is used to assess the rod's behaviour under impact conditions. The numerical investigation is focused on the development of the preliminary FE models. The quasi-static case is used to describe the model calibration methodology. A sensitivity analysis is performed to assess the relative importance of various model parameters followed by an optimization task applied for the model validation.

2. Experimental campaign

Two mechanical test devices have been developed and commissioned for 3-point bending and gravitational impact tests on SNF rod segments. Each fuel rod has been segmented into pieces of ~ 480 mm. The experiments have been conducted in sets of one 3-point bending and one impact test on selected segments of the available PWR SNF rods. The samples have been selected on the base of (near) constant fuel (UO_2), cladding type (Duplex D4) and burnup variation (from 18 to 100 GWd/tHM). The SNF rod segments were pressurized to their corresponding internal pressure, as measured at the end of in-pile service. Further details on sample preparation, device specific characteristics and results with the use of surrogate rods, have been reported in [5,9–13].

In contrast to the 3-point bending tests, the impact tower is not equipped with dedicated sensors for the acquisition of the applied load, sample displacement and pressure. A high-speed camera yields a sequence of high resolution images over a total collection time of around 1 sec. Thus, the mechanical response of the sample is represented by load-deflection curves in the 3-point bending tests, whereas a video illustrates the sample's response in the impact tests. Fig. 1 gives the load-displacement curves of two PWR SNF rod segments with low and high average burnup (BU), during the 3-point bending test. An example of an image sequence during impact is shown in Fig. 2 where a set of frames are selected to illustrate the deflection and fracture of an SNF rod segment. Further details are given in [14].

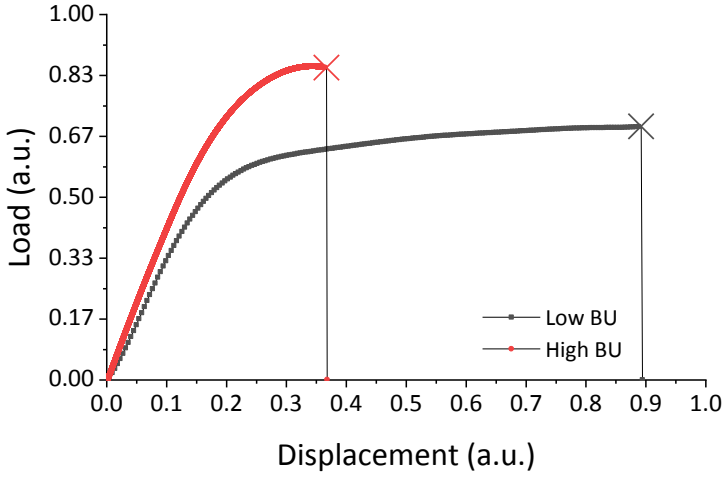

Fig. 1. Load deflection curve of high and low BU samples during the 3-point bending test.

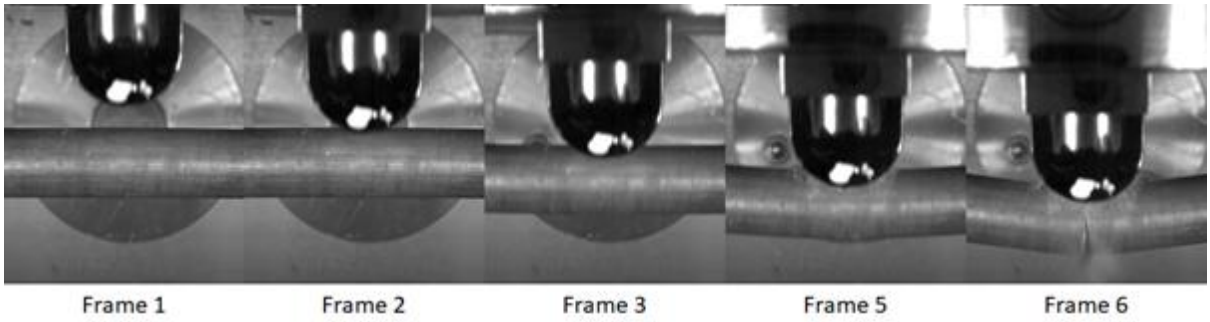

Fig. 2. Representative selected frames of the image sequence during an impact test.

3. Image analysis

Even simple inspection of the sample deflection with time provides extremely valuable understanding of various phenomena that develop when a dynamic load is applied to an SNF rod [14]. Nevertheless, a dedicated effort has been given to develop an image analysis procedure to convert the obtained impact sequence images into convenient data, namely instantaneous sample deflection and impactor velocity per frame (i.e. time). Such analysis is of paramount importance since it provides (a) the means to compare material properties of SNF rods against strain rate (correlation to quasi-static case) and (b) the essential input needed for the FE model calibration against the experimental results.

3.1 Methodology description

The development of the image analysis demanded an unconventional effort , since it was not foreseen at the outset [13], so both the hardware setup and the camera specifications are not fully optimized for this type of data extraction. Concomitant deficiencies had to be overcome by other means. The optimisation of this procedure is currently ongoing, aiming to the determination of the hammer's kinetic energy, acceleration and impact loads, being these achievable on the base of current progresses. The following describes the assumptions made for the development of the methodology along with preliminary results.

The sample's deflection can be calculated by tracking a distinct object (a designated mark) at the front view of the impactor. This object is hand-drawn in Figure 2 and has an irregular white shape against a black background. This approach relies on a major, but realistic, assumption, namely that *the sample moves/deflects (at the symmetry plane) at the same rate as the object on the impactor, independently of its position with regard to the symmetry plane*. In other words, we assume the same directional velocity for the points A and B, as shown in Fig. 3a, which could be located at different axial positions on the cladding.

Of course, this approach also assumes stress equilibrium along the sample, which might not be valid for stiff materials (like SNF rods) and at the early stages of high strain deformations (which exist during an impact test). In truth, of course, this approach calculates the impactor's displacement rather than the sample's deflection. Recent studies have proven that the loading point velocity and the velocities of points along the symmetry plane of the sample can vary slightly [15], but the frequency used to acquire the images is low, and the assumption of established stress equilibrium should be valid.

The image analysis of the video frames is divided in two separate, but equally important, domains:

1. Spatial calibration of the impact sequence images, and
2. Object tracking performed through dedicated image analysis software (Image-Pro Plus).

The obtained images provide a 2-D projection of the 3-D space. Thus, a correlation has to be defined to map geometrically each point onto the image plane. This process is referred to as image calibration and provides a correlation between pixel position into "real-world" dimensions of the experimental device.

The object tracking (using "Image-Pro Plus") gives the position of the tracking object in each single frame. The procedure consists of applying a sequence of filters (optionally) on the selected frames to be examined to enhance the visibility/contrast of the tracking object on the image. Both procedures can be performed independently; but both are essential in the derivation of the final results.

3.2 Applied image calibration

Well-established procedures and dedicated software applications are available to perform image calibration [16]. Unfortunately, since the test rig is already installed at the hot-cell and the potential of image analysis was not foreseen, the application of standard calibration methods is restricted necessitating the development of an alternative method to generate the image calibration of the resulting videos. This method is based on the principle of *utilizing the perspective projection of objects with known dimensions in different positions within the*

acquired image sequence. In other words, since the camera position for each single test is fixed, then the camera parameters can be derived from the dimensions of the dimensionally fully known objects in the images. Considering their length variation with regard to their position in the image, and since all images have the same dimension and camera view, perspective effects are determined and used to correct the original images.

In this case, a sequence of images including static objects was obtained (with the exception of the impactor), which moves along a vertical axis defined by its guiding tube. Fig. 3b provides an understanding of how this movement is projected at a certain frame. To perceive the impactor's position in "pixel" coordinates, the side view of the closed chamber is provided by a cross-section at the symmetry plane of the sample. Three axes are highlighted in black, red and blue giving the movement of the two different planes of the impactor and the symmetry plane of the sample. The calibration was performed by measuring the length variation in each frame of the lower horizontal axis of the impactor located at the plane highlighted in black in Fig. 3b.

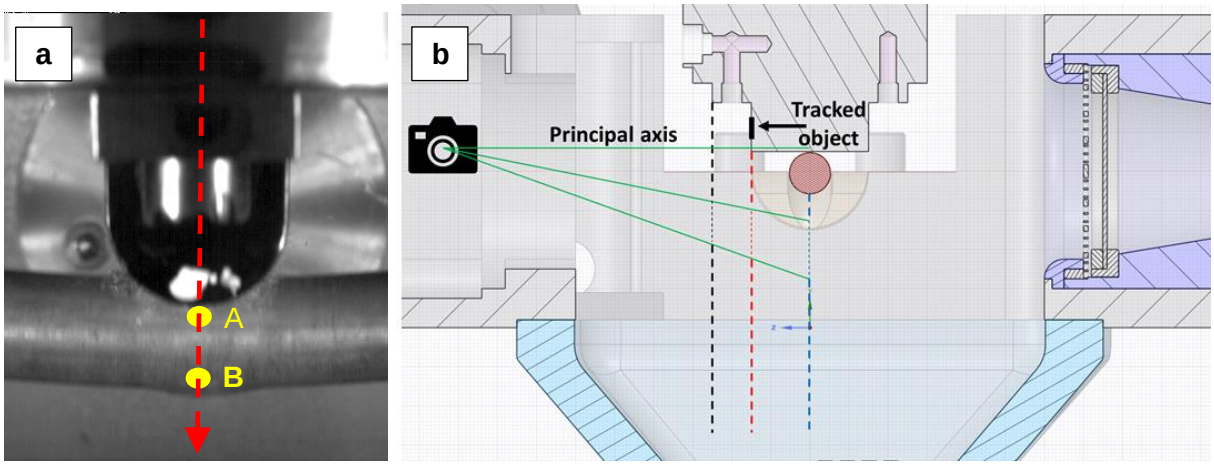

Fig.3. Basic principles on which the image analysis methodology was built. (a) Points A and B are considered to have same directional velocity, (b) side view of the geometrical configuration of the impact tower at a cross-section on the symmetry plane. The effect of the impactor's prospective projection is shown by highlighting axes where the object with known dimensions moves (in red and black).

Upon application of the object tracking algorithm the centroid of the object was calculated in every frame. Therefore, the object tracking method provides results in terms of position in pixels of the centroid of the tracked object per frame. These in turn can be translated to real distance of each point per frame, which are then linearly correlated to the velocity of the hammer.

Typical results of this analysis procedure are presented in Fig. 4. The data points in black represent the hammer's velocity per frame before the application of the spatial calibration (i.e. in a normalised pixel/msec units), while red data points show the converted information in normalised mm/msec units. This representation of the data highlights the effect of the spatial calibration. Subsequently, further characteristic quantities can be derived from these data, i.e. the hammer's instantaneous kinetic energy, acceleration and impact load.

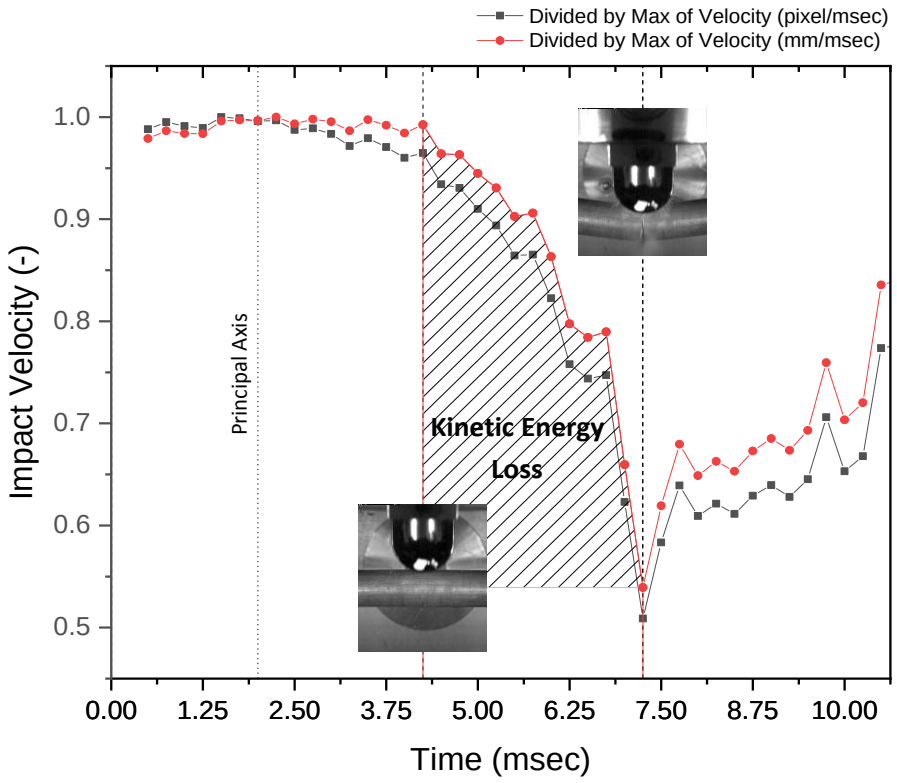

Fig. 4. Camera calibration: Black dots represent raw velocity data of the hammer per frame (normalized by the max velocity in pixel/msec); red dots represent the velocity of the hammer after the spatial calibration has been applied (normalized by the max velocity in mm/msec).

4. Finite Element Modelling

The second part of these investigations concentrates on the modelling of the results using FEA methods, not only to gain a full understanding of the experiments, but also for their verification to assess conditions and configurations outside of the domain defined by the experimental studies themselves. The first phase of the FEA concentrates on rod specific simulation, e.g. the derivation of rod failure criteria, the optimisation of the material models and the examination of the influence of various phenomena (burnup, gap size, strain rate etc.). The second phase focuses on the development of macroscale models to take account of the full SNF assembly with its concomitant structural parts, to investigate its mechanical integrity in various incidental scenarios (transportation shocks/vibration, handling, etc.). Here, the first simplified approach on the model development is described along with first preliminary results.

4.1 Model description

ANSYS Mechanical is used for the development of the FE models. For the quasi-static case (3-point bending), a 3D implicit static structural FE model was developed to simulate the sample deflection when a load is applied by the displacement driver. In contrast, a 3D implicit transient structural analysis is ongoing to simulate the impact sequence where loads are applied by the free fall movement of the impactor.

The pellets are modelled as cylindrical solid elements with a flexible stiffness behaviour [10]. Ceramic materials (pellets) tend to be weak in tension, but strong in compression [17].

Consequently, the ANSYS “cast-iron” material model has been used to describe the pellets constitutive law i.e. it accounts for different plastic yield and hardening in tension and compression while still assuming isotropic elastic behaviour. The cladding has been modelled as a shell element, increasing the integration points than default (to consider plasticity), where the “Voce” law is used to account for non-linear isotropic hardening. The impactor/former and the support were modelled as shell elements with rigid behaviour. At the end of the rod, a point mass has been included in the model to consider inertia effects introduced by the pressure plugs and transducer. This is more relative to the dynamic case. Fracture criteria are not considered at the moment. To minimize computational time the models have been established using 1/4 symmetry.

Pellet dimensions are determined based on typical fabrication data accommodating a well-known swelling rate as a function of burnup. [18,19]. Gravitational acceleration is considered for all bodies. For the quasi-static case, the loads are applied by assigning a maximum displacement at the former in line with the experimental results, while for the dynamic case, an initial velocity is given to the impactor just before impact as derived from the image analysis.

The equivalent (von-Mises) stress distribution at a deflection of 1.5 cm of the cladding at the symmetry z plane for the static configuration is shown in Fig. 5. Although, the model calibration is still ongoing, an immediate qualitative verification with respect to the experimental results is found, as the maximum stresses are developed opposite to the point of impact on the cladding surface in tension, and at a point of the pellet-pellet interface closest to the applied load (symmetry z plane) [11].

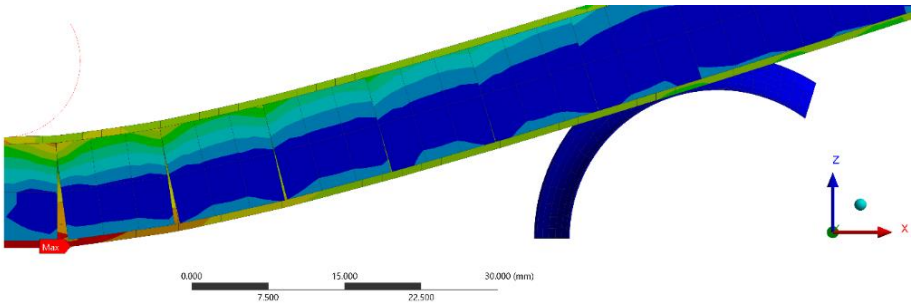

Fig. 5. Equivalent (von-Mises) stresses at a deflection of 1.5 cm of the cladding at the symmetry z plane.

4.2 Model Calibration

The model calibration for the 3-point bending case has been achieved using “optiSLang”, an ANSYS integrated software package for sensitivity analysis and optimization. In short, the FE models are parameterized so that the variation of certain variables (material properties, contact stiffness and type, friction coefficients, etc.) is used to explore their effect on the final results. Then, the numerical results are compared to the experimental data by implementing an objective function which calculates the sum of the squared errors (or differences between experimental and numerical data) over all time steps. Thus, optiSLang explores the cause of non-matching results, to (i) understand the driving parameters, (ii) adjust the parameters for the numerical model and (iii) finally optimize for the specific function of interest.

Due to the modelling complexity of the irradiated cladding/fuel system, the validation was first performed on the experimental data produced with the use of the surrogated rods [5,10]. The

well-known geometrical dimensions and homogeneous mechanical properties of the alumina pellets and used cladding (prior hydrogenation process) can highly simplify the FE models. Therefore, by eliminating a significant number of parameters, the influence of various modelling induced uncertainties (i.e. friction coefficient, contact stiffness and definition, pellet positions) can be assessed. The FE model validated under simplified conditions will be used as the basis for modelling the irradiated fuel/cladding system. Inevitably, further assumptions have to be made due to the highly complex properties and interactions between pellets and cladding. In this case, optiSLang will be used to determine their effective mechanical properties.

OptiSLang produces a so-called “Metamodel of Optimal Prognosis” (MOP) which is a response surface as an explicit function based on the exploration of selected variables. In other words, the MOP is basically the fitted surface created by the response of the most decisive parameters (as derived by optiSLang) of the FEM simulation. Fig. 6a shows an example of an MOP as derived after a sensitivity analysis on the material properties of the model. The data points in red represent how much the simulation deviates from experimental results and the MOP surface is generated using the Isotropic Kriging fitting approach. In this specific case, the effect of the cladding yield stress and Voce exponential coefficient (being the most important parameters in this model) are shown. OptiSLang uses a quality measure, called “Coefficient of Prognosis” (CoP), to evaluate the relative importance of the input variables and to optimize the selection of the MOP. The CoP actually describes the predictive quality of the MOP where high values thereof ensure that the metamodel can be used reliably to explore the solution space, avoiding time-consuming FEM simulation.

Having understood the driving parameters within the model, the next step in the model calibration is to perform an optimisation using the MOP. Now, the parameter range is re-adjusted, and an optimization problem is applied once more to minimize the differences between the numerical and experimental results. Fig 6b gives a series of generated load deflection curves using the model, indicating in black the experimental data, in grey the results from all design inputs to the model and in red the derived optimisation to the experimental data.

The present results are still preliminary in nature and a more detailed parameter space investigation is required to fully assert the accuracy of the model simulations.

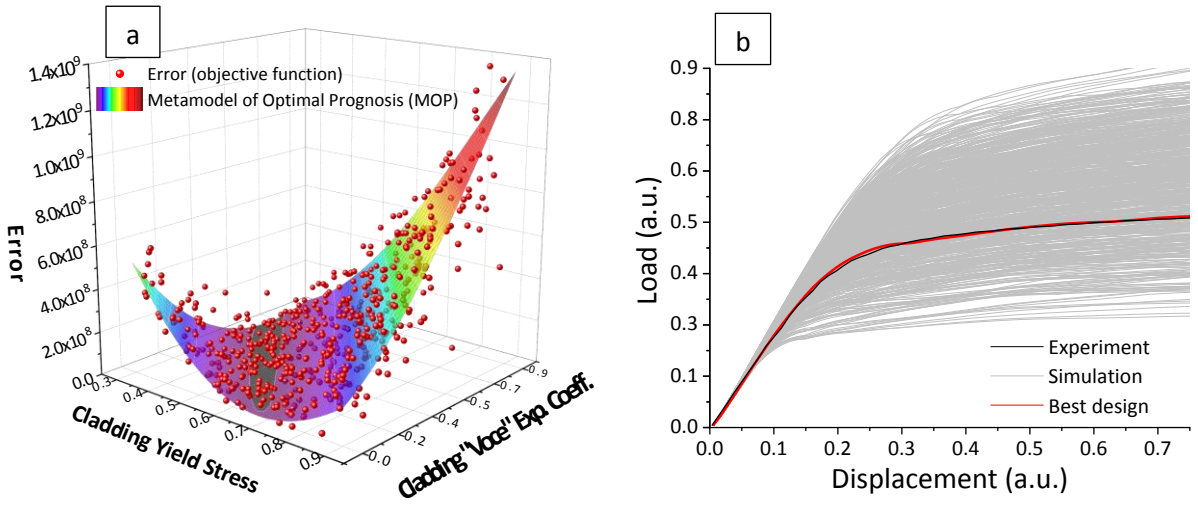

Fig. 6. a) Metamodel of Optimal Prognosis (MOP) representing the most important correlations between parameter input variation and output results. and b) A series of load-deflection simulations (grey) with the experimental data (black) and best fit (red).

5. Conclusions

This paper presents experimental to the numerical investigations on the mechanical response of SNF rods to quasi-static and dynamic loads. Load-deflection curves are generated directly in the 3-point bending tests, whereas in the impact tests, the rod mechanical response is recorded by a high-speed digital camera, which then can be converted to tangible velocity displacement data using an image analysis method. A numerical method using FEA has been developed to describe both experimental arrangements and uses the experimental data for its qualification, enabling it to be used in other domains beyond the experimental regime.

Acknowledgments

This research is partially supported by the Verband Schweizerischer Elektrizitätsunternehmen (VSE-P12). The research benefits of the support of the Gösgen nuclear power plant (KKG) and Framatome GmbH (former AREVA GmbH) who provided and authorised the use of the fuel. We are especially indebted to Dr. Fabian Jatuff, Mr. René Sarrafian and Dr. Bruno Zimmermann from KKG, who greatly contributed to the realisation of this project. Finally, we thank Dr. Elmar Werner Schweitzer and Dr. Klaus Nissen from Framatome GmbH, who constantly give useful insights and comments throughout the phases of this work.

References

[1] IAEA Nuclear Energy Series: Status and Trends in Spent Fuel and Radioactive Waste Management, Vienna, 2018.

[2] Swiss Federal Department of Energy (SFOE), Sectoral plan for deep geological repositories: Conceptual part, Department of Environmen, Transportation, Energy and Communication, Bern, Switzerland, 2008.

[3] B. Hanson, Review of Used Nuclear Fuel Storage and Transportation Technical Gap Analyses, United States of America - Department of Energy, 2012.

[4] D.B. Rigby, Review Board Evaluation of the Technical Basis for Extended Dry Storage and Transportation of Used Nuclear Fuel, United States Nuclear Waste Technical Review Board. (2010) 1–10.

[5] E. Vlassopoulos, S. Caruso, R. Nasyrow, D. Papaioannou, R. Gretter, V. V Rondinella, Nagra Working Rep. NAB 16-067: Investigation of the properties and behaviour of spent nuclear fuel under conditions relevant for interim dry storage, handling and transportation: experimental setup optimisation and cold test campaign, Wettingen, 2017.

[6] K.B. Soreson, J. Kessler, International Perspectives on Technical Data Gaps Associated with Long Term Storage and Transportation of Used Nuclear Fuel Ken Sorenson, in: 11th International Probabilistic Safety Assessment and Management Conference and the Annual European Safety and Reliability Conference 2012 (PSAM11 ESREL 2012), IAPSAM & ESRA, Helsinki, Finland, 2012.

[7] T. Orellana Pérez, H. Völzke, D. Wolff, U. Zencker, Cladding considerations at BAM regarding extended storage of spent fuel, in: Preceedings of the 16th International High-Level Radioactive Waste Management (IHLRWM 2017), American Nuclear Society, Charlotte, NC, 2017.

[8] J. Wang, H. Wang, H. Jiang, B. Bevard, High burn-up spent nuclear fuel transport reliability investigation, Nuclear Engineering and Design. 330 (2018) 497–515. doi:10.1016/j.nucengdes.2018.02.007.

[9] R. Nasyrow, D. Papaioannou, V. V Rondinella, E. Vlassopoulos, K. Linnemann, V. Ballheimer, J. Sterthaus, A. Rolle, F. Wille, S. Caruso, Bending test device for mechanical integrity studies of spent nuclear fuel rods, in: 18th International Symposium on the Packaging and Transportation of Radioactive Materials, PATRAM 2016, Institute of Nuclear Materials Management, Kobe, Japan, 2016.

[10] V. Ballheimer, F. Wille, J. Sterthaus, K. Linnemann, A. Rolle, E. Vlassopoulos, R. Nasyrow, D. Papaioannou, V. V Rondinella, Analysis of parameters affecting the bending behavior of spent fuel rods, in: 18th International Symposium on the Packaging and Transportation of Radioactive Materials, PATRAM 2016, Institute of Nuclear Materials Management, Kobe, Japan, 2016.

[11] E. Vlassopoulos, R. Nasyrow, D. Papaioannou, V.V. Rondinella, S. Caruso, A. Pautz, Destructive tests for determining mechanical integrity of spent nuclear fuel rods, in: ANS IHLRWM 2017 - 16th International High-Level Radioactive Waste Management Conference: Creating a Safe and Secure Energy Future for Generations to Come - Driving Toward Long-Term Storage and Disposal, 2017: pp. 726–733.

[12] V.V. Rondinella, R. Nasyrow, D. Papaioannou, E. Vlassopoulos, F. Cappia, T.A.G. Wiss, O. Dieste-Blanco, Mechanical Integrity Studies on Spent Nuclear Fuel Rods, in: ANS IHLRWM 2017 - 16th International High-Level Radioactive Waste Management Conference: Creating a Safe and Secure Energy Future for Generations to Come - Driving Toward Long-Term Storage and Disposal, American Nuclear Society, Charlotte, NC, United States, 2017: pp. 734–740.

[13] D. Papaioannou, R. Nasyrow, V. V Rondinella, Fuel release experiments on irradiated fuel rodlets under transient impact conditions, Report No: JRC-ITU-TPW-2009/01, Joint Research Centre of the European Commission, 2009.

[14] E. Vlassopoulos, R. Nasyrow, D. Papaioannou, L. Fongaro, R. Gretter, S. Caruso, P. Gretter, J. Somers, V. V. Rondinella, J. Helfenstein, P. Schwizer, Response of Irradiated Nuclear Fuel Rods to Dynamic Loads, Submitted to Kerntechnik. (2018).

[15] B. Koohbor, A. Kidane, M.A. Sutton, X. Zhao, S. Mallon, Analysis of dynamic bending test using ultra high speed DIC and the virtual fields method, International Journal of Impact Engineering. 000 (2017) 1–12. doi:10.1016/j.ijimpeng.2016.12.021.

[16] Single Camera Calibration - MATLAB & Simulink, (n.d.). https://www.mathworks.com/help/vision/ug/single-camera-calibration.html (accessed November 22, 2017).

[17] M. Dallongeville, A. Zeachandirin, P. Purcell, A. Cory, FINITE ELEMENTS ANALYSIS OF INTERGRID BENDING TESTS ON USED FUEL RODS SAMPLES, in: 16th International Symposium on the Packaging and Transportation of Radioactive Materials, PATRAM 2010, n.d.

[18] M. Marchetti, D. Laux, L. Fongaro, T. Wiss, P. Van Uffelen, G. Despaux, V.V. Rondinella, Physical and mechanical characterization of irradiated uranium dioxide with a broad burnup range and different dopants using acoustic microscopy, Journal of Nuclear Materials. 494 (2017) 322–329. doi:10.1016/j.jnucmat.2017.07.041.

[19] J. Spino, J. Rest, W. Goll, C.T. Walker, Matrix swelling rate and cavity volume balance of UO2 fuels at high burn-up, Journal of Nuclear Materials. 346 (2005) 131–144. doi:10.1016/j.jnucmat.2005.06.015.